C. R. Mecanique 346 (2018) 868–876

Contents lists available at ScienceDirect

Comptes Rendus Mecanique

www.sciencedirect.com

Two non-elliptical inhomogeneities with internal uniform stresses interacting with a mode-III crack

Xu Wang [a], Peter Schiavone [b,*]

[a] School of Mechanical and Power Engineering, East China University of Science and Technology, 130 Meilong Road, Shanghai 200237, China
[b] Department of Mechanical Engineering, University of Alberta, 10-203 Donadeo Innovation Centre for Engineering, Edmonton, Alberta T6G 1H9, Canada

ARTICLE INFO

Article history:
Received 22 May 2018
Accepted 11 July 2018
Available online 24 July 2018

Keywords:
Two non-elliptical inhomogeneities
Mode-III crack
Conformal mapping
Cauchy singular integral equation

ABSTRACT

We use the method of Green's functions to analyze an inverse problem in which we aim to identify the shapes of two non-elliptical elastic inhomogeneities, embedded in an infinite matrix subjected to uniform remote stress, which enclose uniform stress distributions despite their interaction with a finite mode-III crack. The problem is reduced to an equivalent Cauchy singular integral equation, which is solved numerically using the Gauss–Chebyshev integration formula. The shapes of the two inhomogeneities and the corresponding location of the crack can then be determined by identifying a conformal mapping composed in part of a real density function obtained from the solution of the aforementioned singular integral equation. Several examples are given to demonstrate the solution.

1. Introduction

The design objective of achieving uniform stress distributions inside multiple non-elliptical elastic inhomogeneities embedded in an infinite elastic matrix has attracted much attention in the literature recently (see, for example, [1–6]). The main reason for such interest lies in the fact that uniform interior stress distributions in embedded inhomogeneities are optimal in that they eliminate the possibility of stress peaks, which are well-known to cause failure of the composite containing the inhomogeneities (for example, in the manufacture of fiber-reinforced composites). In previous studies in this area, the matrix surrounding the inhomogeneities is consistently assumed to be free of any cracks. Naturally, we are led to examine the influence of a cracked matrix on the uniformity of stresses inside multiple embedded inhomogeneities. In a recent seminal study, the authors [7] have established that uniform stresses can still be maintained inside a *single* non-elliptical elastic inhomogeneity interacting with a mode-III finite crack in the matrix when the matrix is subjected to uniform remote stress.

In this work, we extend the study begun in Wang et al. [7] to the uniformity of stresses inside two non-elliptical elastic inhomogeneities interacting with a finite Griffith crack when the matrix is subjected to uniform anti-plane shear stress at infinity. We proceed as follows. By employing a Green's function from a solution derived earlier in Wang and Schiavone [4] (for a screw dislocation interacting with two elastic inhomogeneities with internal uniform stresses), we construct a conformal mapping function and a Cauchy singular integral equation, both of which contain an unknown real

* Corresponding author.
E-mail addresses: xuwang@ecust.edu.cn (X. Wang), p.schiavone@ualberta.ca (P. Schiavone).

https://doi.org/10.1016/j.crme.2018.07.009
1631-0721/

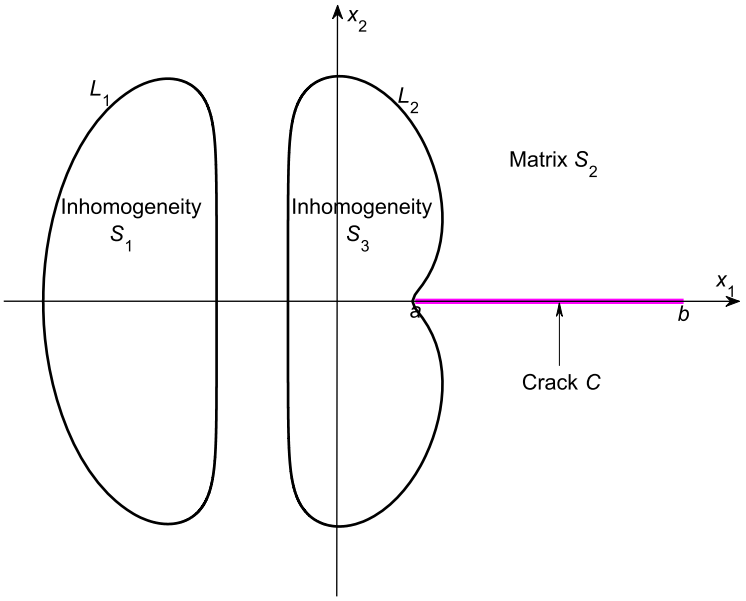

Fig. 1. Two non-elliptical elastic inhomogeneities interacting with a mode-III Griffith crack on the real axis under uniform remote stress σ_{32}^{∞}.

density function. The Cauchy singular integral equation is solved numerically for the real density function by applying the Gauss–Chebyshev integration formula [8], so that the conformal mapping function characterizing the required shapes of the inhomogeneities and the corresponding location of the matrix crack is completely determined. Our analysis indicates that the finite matrix crack plays a key role in the non-elliptical shapes of the two inhomogeneities, whereas it exerts no influence on the internal uniform stresses inside the two inhomogeneities. Several typical examples are presented to demonstrate the solution.

2. Problem formulation

Under anti-plane shear deformations of an isotropic elastic material, the two shear stress components σ_{31} and σ_{32}, the out-of-plane displacement w and the stress function ϕ can be expressed in terms of a single analytic function $f(z)$ of the complex variable $z = x_1 + \mathrm{i}x_2$ as [9]

$$\sigma_{32} + \mathrm{i}\sigma_{31} = \mu f'(z), \qquad \phi + \mathrm{i}\mu w = \mu f(z) \tag{1}$$

where μ is the shear modulus, and the two shear stress components can be expressed in terms of the stress function as [9]

$$\sigma_{32} = \phi_{,1}, \qquad \sigma_{31} = -\phi_{,2} \tag{2}$$

As shown in Fig. 1, we consider two non-elliptical elastic inhomogeneities embedded in an infinite matrix weakened by a traction-free finite Griffith crack $\{a \le x_1 \le b, x_2 = 0^{\pm}\}$ on the real axis. Let S_1, S_2, and S_3 denote the left inhomogeneity, the matrix and the right inhomogeneity, respectively, all of which are perfectly bonded through the left and the right interfaces L_1 and L_2. We denote the crack by C. The matrix is subjected to uniform remote anti-plane shear stress σ_{32}^{∞} (with $\sigma_{31}^{\infty} = 0$). In what follows, the subscripts 1, 2 and 3 are used to identify the respective quantities in S_1, S_2 and S_3. Our objective below is to determine whether uniform stresses continue to exist inside the two non-elliptical inhomogeneities when interacting with the mode-III crack.

3. The shapes of the two inhomogeneities permitting internal uniform stresses

The original interaction problem of the two inhomogeneities and the crack can be formulated as a continuous distribution of screw dislocations on the crack. The solution for a screw dislocation interacting with two non-elliptical elastic inhomogeneities permitting internal uniform stresses was recently derived by Wang and Schiavone [4]. By employing this solution as a Green's function, the following conformal mapping function for the present interaction problem can be constructed,

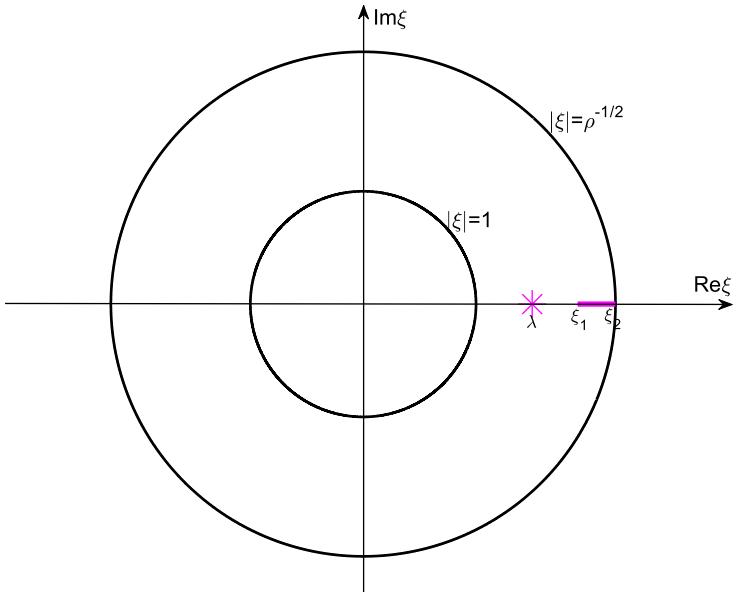

Fig. 2. The problem in the ξ-plane.

$$z=\omega(\xi)=R\left[\begin{array}{l}\frac{1}{\xi-\lambda}+\frac{p}{\xi-\lambda^{-1}}+\frac{\Lambda^{-1}p}{\rho\xi-\lambda^{-1}}+\sum_{n=1}^{+\infty}(\frac{\lambda^{-n-1}+p\Lambda^{-1}\rho^{n}\lambda^{n+1}}{1-\Lambda\rho^{-n}}\xi^{n}+\frac{\lambda^{n-1}+p\lambda^{1-n}}{\Lambda^{-1}\rho^{-n}-1}\xi^{-n})\\ +\int_{\xi_1}^{\xi_2}q(\eta)[\ln\frac{\xi-\eta^{-1}}{\xi-\lambda^{-1}}+\Lambda^{-1}\ln\frac{\rho\xi-\eta^{-1}}{\rho\xi-\lambda^{-1}}+\sum_{n=1}^{+\infty}\frac{1}{n}(\frac{\Lambda^{-1}\rho^{n}\eta^{n}\xi^{n}}{1-\Lambda\rho^{-n}}-\frac{\eta^{-n}\xi^{-n}}{\Lambda^{-1}\rho^{-n}-1})]\mathrm{d}\eta\end{array}\right] \tag{3}$$

$$\xi(z)=\omega^{-1}(z),\quad 1\le|\xi|\le\rho^{-\frac{1}{2}}$$

where R is a real scaling constant, p and λ $(1<\lambda<\rho^{-\frac{1}{2}})$ are two real constants, $q(\eta)$ is a real density function to be determined, and

$$\xi_1=\omega^{-1}(b),\qquad \xi_2=\omega^{-1}(a),\qquad \xi_1<\xi_2 \tag{4}$$

$$\Gamma_1=\frac{\mu_1}{\mu_2},\qquad \Gamma_3=\frac{\mu_3}{\mu_2},\qquad \Lambda=\frac{(\Gamma_1+1)(\Gamma_3-1)}{(\Gamma_1-1)(\Gamma_3+1)} \tag{5}$$

Using the mapping function in Eq. (3), the matrix S_2 in the z-plane is mapped onto an annulus $1\le|\xi|\le\rho^{-\frac{1}{2}}$ in the ξ-plane, the interfaces L_1 and L_2 in the z-plane are mapped onto two co-axial circles with the radii 1 and $\rho^{-\frac{1}{2}}$ in the ξ-plane respectively, the finite Griffith crack C in the z-plane is mapped onto the slit $\{\xi_1\le\mathrm{Re}\{\xi\}\le\xi_2,\mathrm{Im}\{\xi\}=0^{\pm}\}$ in the ξ-plane, and the point $z=\infty$ is mapped to $\xi=\lambda$ (see Fig. 2).

In addition, the following Cauchy singular integral equation is obtained as a condition that ensures that the crack faces are traction-free:

$$\begin{aligned}&\int_{\xi_1}^{\xi_2}\frac{q(\eta)}{\xi-\eta}\mathrm{d}\eta+\int_{\xi_1}^{\xi_2}q(\eta)\left\{\frac{1}{\Lambda(\xi-\rho\eta)}+\frac{1}{K(\xi-\eta^{-1})}+\frac{\rho}{K\Lambda(\rho\xi-\eta^{-1})}\right.\\&\qquad\left.+\sum_{n=1}^{+\infty}\left[\frac{\eta^{n}(K^{-1}\xi^{n-1}-\xi^{-n-1})}{\Lambda\rho^{-n}(1-\Lambda\rho^{-n})}+\frac{K^{-1}\xi^{-n-1}-\xi^{n-1}}{\eta^{n}(\Lambda^{-1}\rho^{-n}-1)}\right]\right\}\mathrm{d}\eta\\&=\frac{1-pK\lambda^{2}}{K(\xi-\lambda)^{2}}+\frac{p\lambda^{2}-K}{K(\lambda\xi-1)^{2}}+\frac{\Lambda^{-1}\rho p}{K(\rho\xi-\lambda^{-1})^{2}}-\frac{\Lambda^{-1}\rho p}{(\lambda^{-1}\xi-\rho)^{2}}\\&\qquad+\sum_{n=1}^{+\infty}n\left[\frac{(\lambda^{-n-1}+p\Lambda^{-1}\rho^{n}\lambda^{n+1})(\xi^{-n-1}-K^{-1}\xi^{n-1})}{1-\Lambda\rho^{-n}}+\frac{(\lambda^{n-1}+p\lambda^{1-n})(K^{-1}\xi^{-n-1}-\xi^{n-1})}{\Lambda^{-1}\rho^{-n}-1}\right],\quad \xi_1<\xi<\xi_2\\&\int_{\xi_1}^{\xi_2}q(\eta)\mathrm{d}\eta=0\end{aligned} \tag{6}$$

where the mismatch parameter K is defined by

$$K = \frac{\Gamma_1 - 1}{\Gamma_1 + 1}, \quad -1 \le K \le 1 \tag{7}$$

It should be noted that the constraint in Eq. $(6)_2$ has been utilized to derive Eqs. (3) and $(6)_1$. The singular integral equation in Eq. (6) can be solved numerically through normalization and utilization of the Gauss–Chebyshev integration formula [8]. Once Eq. (6) is solved, the term containing the real density function $q(\eta)$ in Eq. (3) can then also be evaluated (quite expediently) using the Gauss–Chebyshev integration formula so that the corresponding mapping function is known completely. Consequently, the shapes of the two inhomogeneities and the location of the crack can be determined. Apparently, the stresses continue to exhibit the strong square root singularity at the crack tips.

In addition, the three analytic functions for the present interaction problem are given by

$$f_1(z) = \frac{2k}{\Gamma_1 + 1} z + 2c_1, \quad z \in S_1 \tag{8}$$

$$f_3(z) = \frac{2k}{\Gamma_3 + 1} z + 2c_3, \quad z \in S_3 \tag{9}$$

$$\begin{aligned} f_2(\xi) &= f_2\big(\omega(\xi)\big) = k\omega(\xi) + \frac{k(\Gamma_1 - 1)}{\Gamma_1 + 1}\bar{\omega}\left(\frac{1}{\xi}\right) + c_1(\Gamma_1 + 1) + \bar{c}_1(\Gamma_1 - 1) \\ &= k\omega(\xi) + \frac{k(\Gamma_3 - 1)}{\Gamma_3 + 1}\bar{\omega}\left(\frac{1}{\rho\xi}\right) + c_3(\Gamma_3 + 1) + \bar{c}_3(\Gamma_3 - 1), \quad 1 \le |\xi| \le \rho^{-\frac{1}{2}} \end{aligned} \tag{10}$$

where c_1 and c_3 are complex constants, and

$$k = \frac{\sigma_{32}^{\infty}(\Gamma_1 + 1)}{\mu_2[\Gamma_1 + 1 - p\lambda^2(\Gamma_1 - 1)]} \tag{11}$$

Thus, it follows from Eqs. (1), (8) and (9) that the stresses are uniformly distributed inside the two inhomogeneities as follows

$$\begin{aligned} \sigma_{32} &= \frac{2\Gamma_1\sigma_{32}^{\infty}}{\Gamma_1 + 1 - p\lambda^2(\Gamma_1 - 1)}, \qquad \sigma_{31} = 0, \quad z \in S_1 \\ \sigma_{32} &= \frac{2\Gamma_3(\Gamma_1 + 1)\sigma_{32}^{\infty}}{(\Gamma_3 + 1)[\Gamma_1 + 1 - p\lambda^2(\Gamma_1 - 1)]} = \frac{2\Gamma_3\sigma_{32}^{\infty}}{\Gamma_3 + 1 - p\lambda^2\Lambda^{-1}(\Gamma_3 - 1)}, \qquad \sigma_{31} = 0, \quad z \in S_3 \end{aligned} \tag{12}$$

which are unaffected by the nearby crack.

4. Illustrative examples

In this section, the shapes of the two inhomogeneities and the location of the crack will be determined for given values of the seven real parameters Λ, ρ, λ, K, p, ξ_1, and ξ_2.

In the first example, we choose:

$$\Lambda = 1, \qquad \rho = 0.2, \qquad \lambda = \rho^{-\frac{1}{4}} = 1.4953, \qquad K = -0.5, \qquad p = 0.25, \qquad \xi_1 = 1.9, \qquad \xi_2 = 2.235 \tag{13}$$

In this example, both inhomogeneities are softer than the matrix ($\Gamma_1 = \Gamma_3 = 1/3$). The shapes of the two inhomogeneities and the location of the crack are shown in Fig. 3. We can see from Fig. 3 that the shape of the left inhomogeneity is affected only minimally, whereas that of the right inhomogeneity is apparently altered quite significantly by the crack, which is located on the right-hand side of the right inhomogeneity. The right inhomogeneity becomes non-convex, with its area reduced by the influence of the nearby crack.

In the second example, we choose:

$$\begin{aligned} &\Lambda = 1, \qquad \rho = 0.2, \qquad \lambda = \rho^{-\frac{1}{4}} = 1.4953, \qquad K = -0.5, \qquad p = 0.25 \\ &\xi_1 = -2.18, \qquad \xi_2 = \rho^{-\frac{1}{2}}/\xi_1 = -1.0257 \end{aligned} \tag{14}$$

In this example, both inhomogeneities are again softer than the matrix. The shapes of the two inhomogeneities and the location of the crack are shown in Fig. 4. It is observed from Fig. 4 that the shapes and sizes of the two inhomogeneities are identical, and that one inhomogeneity is simply a mirror image of the other with respect to the vertical line $x_1 = \frac{1}{2}(a + b)$. The shapes of both inhomogeneities are apparently affected by the crack lying between them. Both inhomogeneities become non-convex due to the influence of the nearby crack.

In the third example, we choose:

$$\Lambda = 1, \qquad \rho = 0.2, \qquad \lambda = \rho^{-\frac{1}{4}} = 1.4953, \qquad K = 0.5, \qquad p = 0.25, \qquad \xi_1 = 1.82, \qquad \xi_2 = 2.22 \tag{15}$$

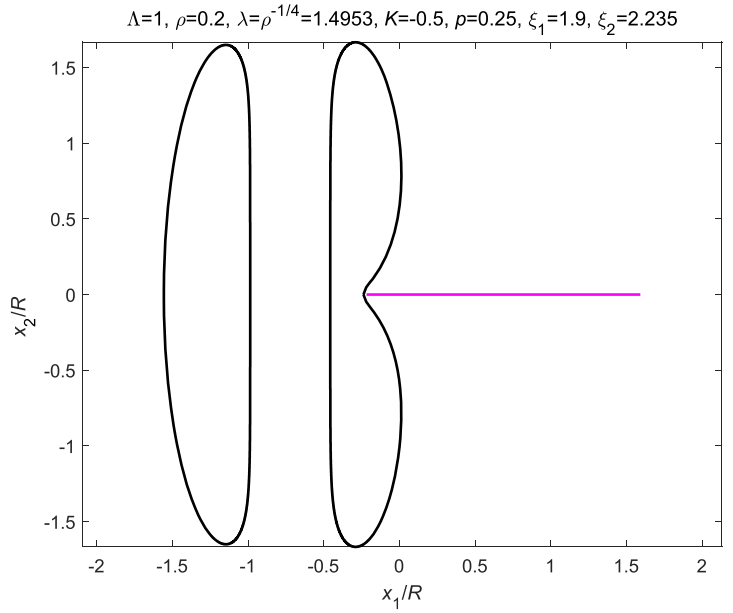

Fig. 3. The non-elliptical shapes of the two inhomogeneities and the location of the crack by choosing the seven parameters in Eq. (13).

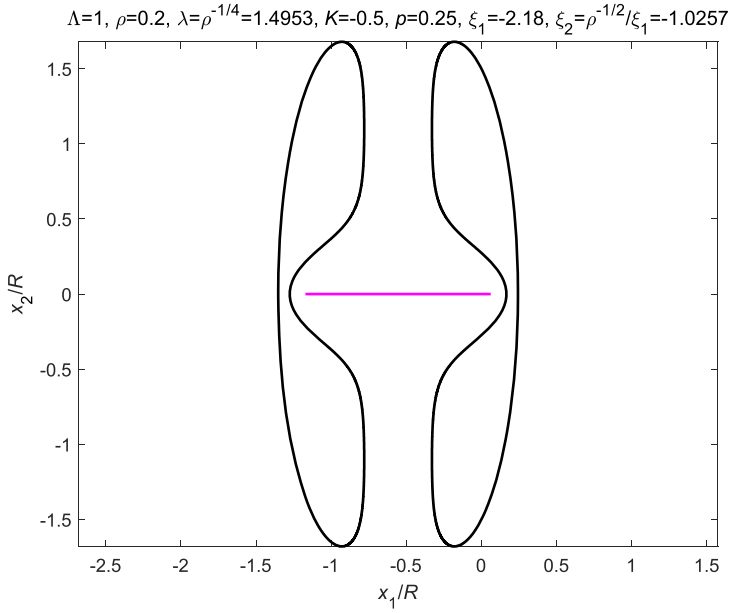

Fig. 4. The non-elliptical shapes of the two inhomogeneities and the location of the crack by choosing the seven parameters in Eq. (14).

In this example, both inhomogeneities are stiffer than the matrix ($\Gamma_1 = \Gamma_3 = 3$). The shapes of the two inhomogeneities and the location of the crack are shown in Fig. 5. We can see from Fig. 5 that the shape of the left inhomogeneity is affected only marginally, whereas that of the right inhomogeneity is indeed altered by the crack, which is located on the right-hand side of the right inhomogeneity. The area of the right inhomogeneity is enlarged and a corner is formed on the boundary of the right inhomogeneity as a result of the influence of the nearby crack.

In the fourth example, we choose

$$\begin{aligned} &\Lambda = 1, \qquad \rho = 0.2, \qquad \lambda = \rho^{-\frac{1}{4}} = 1.4953, \qquad K = 0.5, \qquad p = 0.25 \\ &\xi_1 = -2.15, \qquad \xi_2 = \rho^{-\frac{1}{2}}/\xi_1 = -1.04 \end{aligned} \tag{16}$$

In this example, both inhomogeneities are again stiffer than the matrix. The shapes of the two inhomogeneities and the location of the crack are shown in Fig. 6. It is observed from Fig. 6 that one inhomogeneity is again simply a mirror image

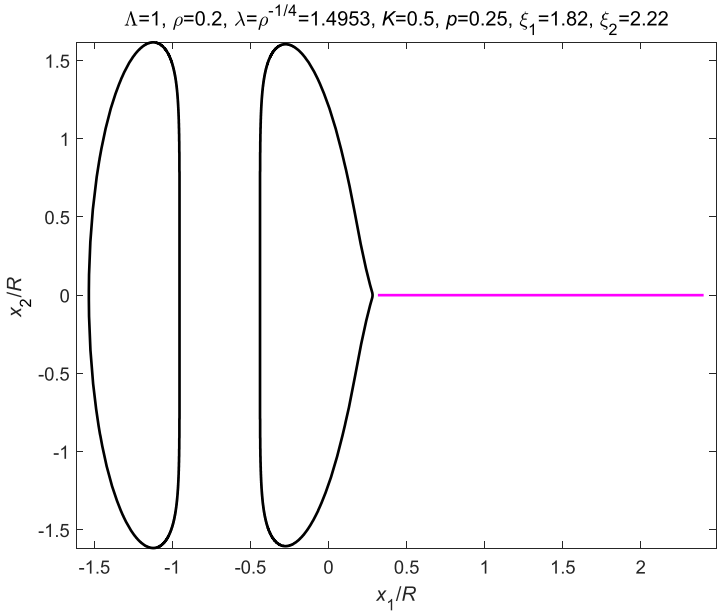

Fig. 5. The non-elliptical shapes of the two inhomogeneities and the location of the crack by choosing the seven parameters in Eq. (15).

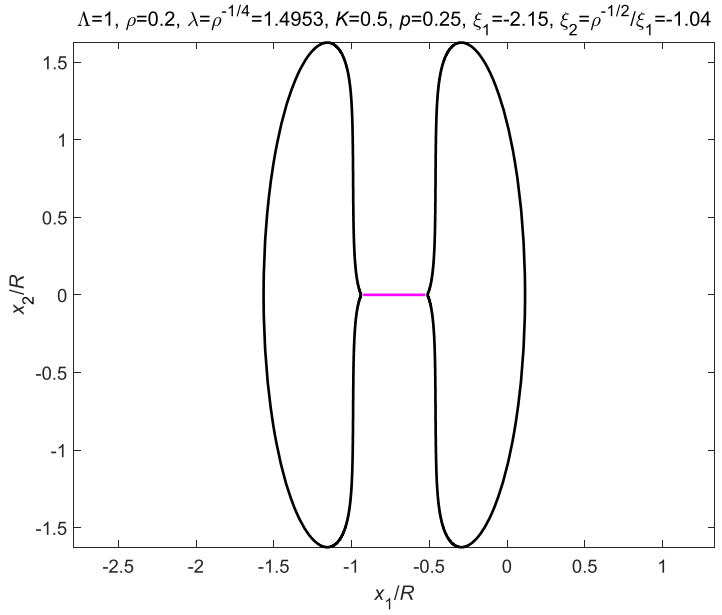

Fig. 6. The non-elliptical shapes of the two inhomogeneities and the location of the crack by choosing the seven parameters in Eq. (16).

of the other with respect to the vertical line $x_1 = \frac{1}{2}(a+b)$. The shapes of both inhomogeneities are clearly affected by the crack lying between them, with two corners formed on the boundaries of the two inhomogeneities.

In the fifth example, we choose:

$$\Lambda = -1, \qquad \rho = 0.05, \qquad \lambda = \rho^{-\frac{1}{4}} = 2.1147, \qquad K = 0.5, \qquad p = 0.1, \qquad \xi_1 = 3.2, \qquad \xi_2 = 4.47 \tag{17}$$

In this example, the left inhomogeneity is stiffer, but the right inhomogeneity is softer than the matrix ($\Gamma_1 = 3$, $\Gamma_3 = 1/3$). The shapes of the two inhomogeneities and the location of the crack are shown in Fig. 7. We see that the right portion of the right inhomogeneity is again affected by the crack, with the right inhomogeneity becoming non-convex.

In the sixth example, we choose:

$$\Lambda = -1, \qquad \rho = 0.05, \qquad \lambda = \rho^{-\frac{1}{4}} = 2.1147, \qquad K = 0.5, \qquad p = 0.1, \qquad \xi_1 = 1.01, \qquad \xi_2 = 1.4 \tag{18}$$

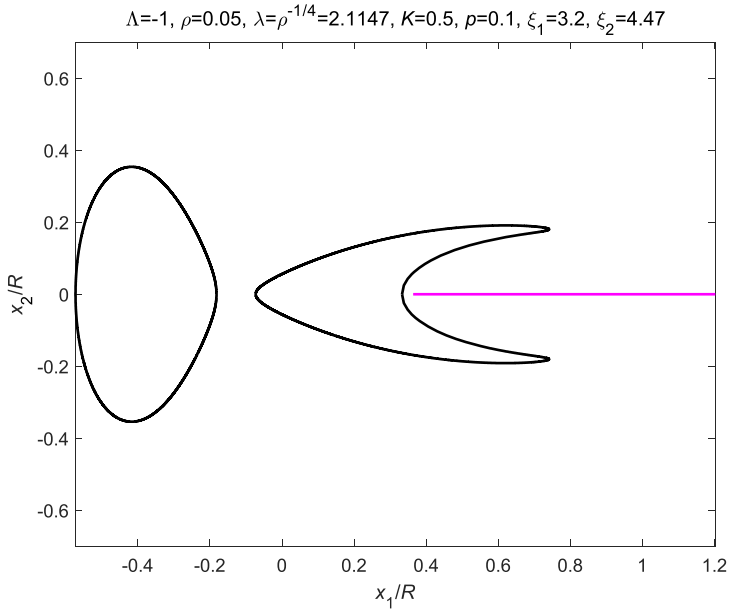

Fig. 7. The non-elliptical shapes of the two inhomogeneities and the location of the crack by choosing the seven parameters in Eq. (17).

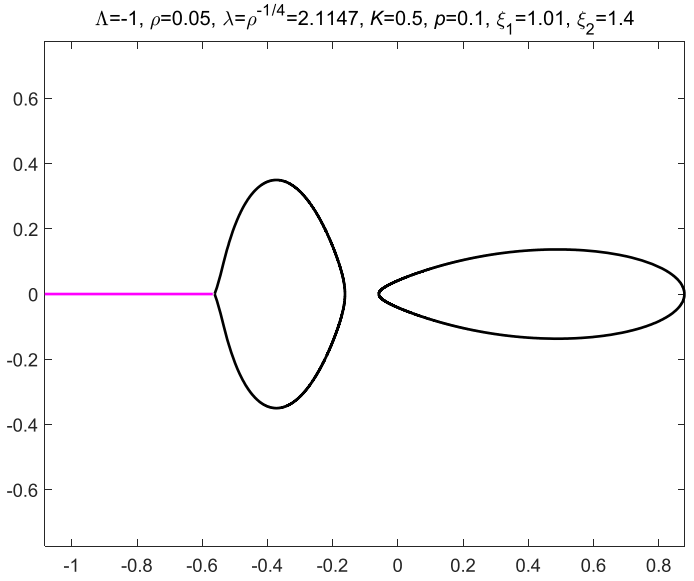

Fig. 8. The non-elliptical shapes of the two inhomogeneities and the location of the crack by choosing the seven parameters in Eq. (18).

In this example, we again have the left inhomogeneity stiffer, but the right inhomogeneity softer than the matrix. The shapes of the two inhomogeneities and the location of the crack are shown in Fig. 8. We see that the left portion of the left inhomogeneity is again affected by the crack. The area of the left inhomogeneity is enlarged, and a corner is formed on the boundary of the left inhomogeneity as a result of the influence of the nearby crack.

In the seventh example, we choose:

$$\Lambda = -1, \qquad \rho = 0.05, \qquad \lambda = \rho^{-\frac{1}{4}} = 2.1147, \qquad K = 0.5, \qquad p = 0.1, \qquad \xi_1 = -4, \qquad \xi_2 = -1.3 \tag{19}$$

In this example, we again have the left inhomogeneity stiffer, but the right inhomogeneity softer than the matrix. The shapes of the two inhomogeneities and the location of the crack are shown in Fig. 9. It is observed from Fig. 9 that the right portion of the left inhomogeneity and the left portion of the right inhomogeneity are clearly affected by the nearby crack that lies between the two inhomogeneities. A corner is formed on the boundary of the left inhomogeneity, whilst the right inhomogeneity becomes non-convex.

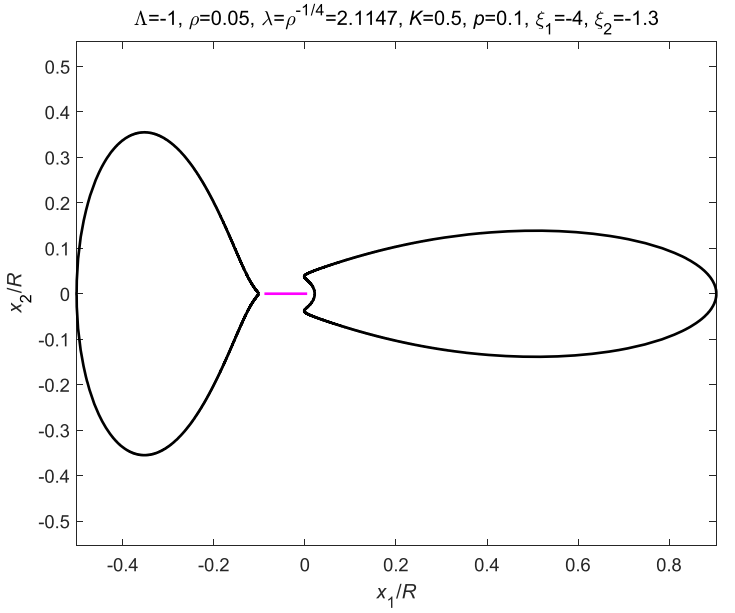

Fig. 9. The non-elliptical shapes of the two inhomogeneities and the location of the crack by choosing the seven parameters in Eq. (19).

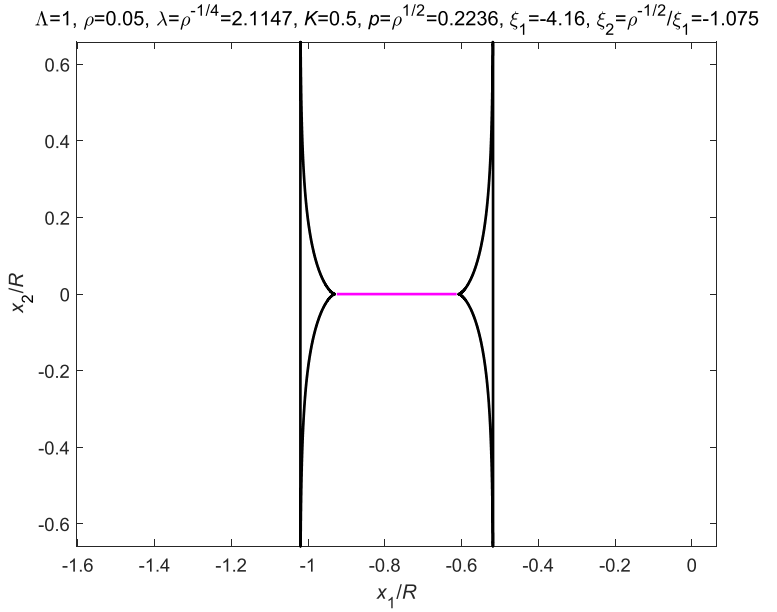

Fig. 10. The non-elliptical shapes of the two inhomogeneities and the location of the crack by choosing the seven parameters in Eq. (20).

In the final example, we choose:

$$\begin{aligned} &\Lambda = 1, \qquad \rho = 0.05, \qquad \lambda = \rho^{-\frac{1}{4}} = 2.1147, \qquad K = 0.5, \qquad p = \rho^{\frac{1}{2}} = 0.2236 \\ &\xi_1 = -4.16, \qquad \xi_2 = \rho^{-\frac{1}{2}}/\xi_1 = -1.075 \end{aligned} \tag{20}$$

In this example, both the inhomogeneities are stiffer than the matrix. The shapes of the two inhomogeneities and the location of the crack are shown in Fig. 10. In this extreme case (as illustrated in Fig. 10) there are three sharp corners on the boundary of each inhomogeneity, which are again mirror images of each other with respect to the vertical line $x_1 = \frac{1}{2}(a+b)$. It is seen from Eq. (10) that the stresses in the matrix are bounded at these sharp corners on the boundaries of the two inhomogeneities and that they exhibit the square root singularity only at the two crack tips.

The numerical results presented in this section clearly indicate that the crack exerts a significant influence on the shapes of inhomogeneities permitting internal uniform stress distributions.

5. Conclusions

In this work, we prove that the internal stresses inside two non-elliptical inhomogeneities interacting with a mode-III crack under uniform anti-plane shear stress at infinity can indeed be maintained uniform despite the presence of the crack. The internal stresses inside the two inhomogeneities given by Eq. (12) are independent of the existence of the crack, whereas the non-elliptical shapes of the two inhomogeneities are significantly influenced by the nearby crack. The non-elliptical shapes of the two inhomogeneities are caused by two factors: one is the interaction between the two inhomogeneities themselves (even in the absence of the crack), the other is the influence of the crack. Our solution method can be conveniently modified to study the uniformity of stresses inside two non-elliptical inhomogeneities interacting with a Zener–Stroh crack loaded by a net screw dislocation Burgers vector. Furthermore, the uniformity property inside the two inhomogeneities interacting with a mode-III crack continues to hold when the remote loading is non-uniform. In the case of arbitrary non-uniform remote loading, the conformal mapping function in Eq. (3) should be reconstructed and higher-order poles (instead of first-order poles) added at $\xi = \lambda^{-1}$ and $\xi = \rho^{-1}\lambda^{-1}$ outside the annulus $1 \leq |\xi| \leq \rho^{-\frac{1}{2}}$ to account for the non-uniform loading at infinity.

Acknowledgements

This work is supported by the National Natural Science Foundation of China (Grant No. 11272121) and through a Discovery Grant from the Natural Sciences and Engineering Research Council of Canada (Grant No. RGPIN – 2017-03716115112).

References

[1] H. Kang, E. Kim, G.W. Milton, Inclusion pairs satisfying Eshelby's uniformity property, SIAM J. Appl. Math. 69 (2008) 577–595.
[2] L.P. Liu, Solution to the Eshelby conjectures, Proc. R. Soc. Lond. A 464 (2008) 573–594.
[3] X. Wang, Uniform fields inside two non-elliptical inclusions, Math. Mech. Solids 17 (2012) 736–761.
[4] X. Wang, P. Schiavone, Two inhomogeneities of irregular shape with internal uniform stress fields interacting with a screw dislocation, C. R. Mecanique 344 (2016) 532–538.
[5] M. Dai, C.F. Gao, C.Q. Ru, Uniform stress fields inside multiple inclusions in an elastic infinite plane under plane deformation, Proc. R. Soc. Lond. A 471 (2015) 20140933.
[6] M. Dai, C.Q. Ru, C.F. Gao, Uniform strain fields inside multiple inclusions in an elastic infinite plane under anti-plane shear, Math. Mech. Solids 22 (2017) 117–128.
[7] X. Wang, L. Chen, P. Schiavone, Uniformity of stresses inside a non-elliptical inhomogeneity interacting with a mode III crack, submitted for publication.
[8] F. Erdogan, G.D. Gupta, On the numerical solution of singular integral equations, Q. Appl. Math. 29 (1972) 525–534.
[9] T.C.T. Ting, Anisotropic Elasticity—Theory and Applications, Oxford University Press, New York, 1996.